Gilbert Damping Parameter in MgO-Based Magnetic Tunnel Junctions from First Principles

Hui-Min Tang[1] and Ke Xia[1,2,*]

[1] *The Center for Advanced Quantum Studies and Department of Physics, Beijing Normal University, Beijing 100875, China*

[2] *Synergetic Innovation Center for Quantum Effects and Applications (SICQEA), Hunan Normal University, Changsha 410081, China*

(Received 26 November 2016; revised manuscript received 14 February 2017; published 6 March 2017)

We perform a first-principles study of the Gilbert damping parameter (α) in normal-metal/MgO-cap/ferromagnet/MgO-barrier/ferromagnetic magnetic tunnel junctions. The damping is enhanced by interface spin pumping, which can be parametrized by the spin-mixing conductance ($G^{\uparrow\downarrow}$). The calculated dependence of Gilbert damping on the thickness of the MgO capping layer is consistent with experiment and indicates that the decreases in α with increasing thickness of the MgO capping layer is caused by suppression of spin pumping. Smaller α can be achieved by using a clean interface and alloys. For a thick MgO capping layer, the imaginary part of the spin-mixing conductance nearly equals the real part, and the large imaginary mixing conductance implies that the change in the frequency of ferromagnetic resonance can be observed experimentally. The normal-metal cap significantly affects the Gilbert damping.

DOI: 10.1103/PhysRevApplied.7.034004

I. INTRODUCTION

Magnetic tunnel junctions (MTJs) with an epitaxial (001)-oriented MgO barrier exhibit a large tunnel magnetoresistance ratio (TMR) at room temperature, which makes them a good candidate for applications in magnetic devices [1–6]. Apart from this large TMR ratio, perpendicular magnetic anisotropy (PMA) and magnetic damping (α) in CoFeB/MgO/CoFeB MTJs have been investigated in detailed studies [7–10]. The MTJ is a promising candidate as memory cells in spin-transfer-torque magnetic random-access memory (STT MRAM) because of their high thermal stability, low STT switching current, and high magnetoresistance (MR). To produce STT MRAM with long retention time [11] as well as spin-torque oscillators and diodes with stable precession [12–14], a larger PMA is necessary. In addition, the switching current in STT-based devices is proportional to α [15–20], so a small α is desired.

Recent experiments show that using a MgO capping layer on CoFeB/MgO/CoFeB (or FeB) MTJs can increase the PMA and decrease α [21–24]. Though thickening the MgO capping layer decreases α and increases the PMA, it also decreases the TMR [25], so a moderately thick MgO capping layer is preferable. Tsunegi *et al.* [22] found $\alpha \sim 0.0054$ and PMA ~ 3.3 erg/cm^2 in a MgO-barrier/FeB/MgO-cap structure with a 0.6-nm MgO capping layer using the spin-torque diode effect. The decreases in α appear to come from suppression of spin pumping [26,27] at the ferromagnet–normal-metal (FM/NM) interface [21]. However, Moriyama *et al.* [28] measured a large voltage signal in MTJs with an Al_2O_3 tunnel barrier, a behavior which cannot be explained by the spin-pumping mechanism. It is not clear whether spin-pumping theory is applicable to MgO-based tunnel junctions.

Here, we use first-principles calculations to analyze the relation between α and spin pumping in NM/MgO/FM MTJs. Our calculated α estimated from $G^{\uparrow\downarrow}$ agrees well with the experiment [13], and the imaginary part of $G^{\uparrow\downarrow}$ ($G_i^{\uparrow\downarrow}$) almost equals the real part ($G_r^{\uparrow\downarrow}$), especially with a thick MgO capping layer. These results indicate that the decrease in α comes from the suppression of spin pumping, and the large $G_i^{\uparrow\downarrow}$ implies that the change in frequency of the ferromagnetic resonance can be observed experimentally. A clean interface and an alloy electrode promote small α. Moreover, we find that the capping normal metal greatly affects α.

This article is organized as follows. In Sec. II, we introduce scattering theory in order to estimate α by the parameter $G^{\uparrow\downarrow}$. In Sec. III, we present our results of α in NM/MgO/FM MTJs. Section IV is our summary.

II. SPIN PUMPING AND GILBERT DAMPING PARAMETER

For a FM/NM interface, the magnetization in the FM layer can be simplified as a macrospin $\mathbf{M} = M_s V \mathbf{m}$, where $\mathbf{m}$ is the unit vector, M_s is the saturation magnetization, and V is the total FM volume. When the magnetization processes, a spin current $\mathbf{I}_s^{\mathrm{pump}}$ is pumped out of the ferromagnet [26]:

$$\mathbf{I}_s^{\mathrm{pump}}(t) = \frac{\hbar}{4\pi}[G_r^{\uparrow\downarrow}\mathbf{m}(t) \times \dot{\mathbf{m}} + G_i^{\uparrow\downarrow}\dot{\mathbf{m}}(t)], \qquad (1)$$

where $G^{\uparrow\downarrow} = (e^2/h)\mathrm{Tr}(\mathbf{I} - \mathbf{r}_\uparrow^\dagger \mathbf{r}_\downarrow)$ is the spin-mixing conductance, and $\mathbf{I}$ and $\mathbf{r}_\sigma$ are the unit matrix and the matrix of interface reflection coefficients for spin σ spanned by the scattering channels at the Fermi energy [29].

*kexia@bnu.edu.cn

An immediate consequence of the spin pump is enhanced Gilbert damping of the magnetization dynamics [26]. When the NM is an ideal spin sink, the spin backflow can be disregarded, and by the conservation of the spin angular momentum, enhanced Gilbert damping can be obtained [30]

$$\alpha = \frac{\gamma\hbar}{4\pi M_s V}\int dE\left(-\frac{df}{dE}\right)G_r^{\uparrow\downarrow}(E), \tag{2}$$

where γ is the gyromagnetic ratio. At finite temperature, the volume V is replaced by the magnetic coherent volume V_a [31,32]. The temperature effects contain two factors: one is the Fermi-Dirac distribution function $f = \exp\{[(E-E_f)/K_BT] + 1\}^{-1}$, and the other is the magnetic coherent volume $V_a = \{2/[3\xi(5/2)]\}[(4\pi D)/(k_BT)]^{3/2}$, where ξ is the Riemann ζ function, T is the ambient temperature, and D is the spin stiffness constant. At 0 K, V_a equals V and $-\partial f/\partial E$ is reduced to the δ function $\delta(E-E_f)$ at the Fermi level E_f. In general, the total Gilbert damping contains the bulk part α_0 and the interface enhancement part α. In Konoto *et al.*'s [21] experiment, α_0 accounts for 40% of the total Gilbert damping; however, the decreases in Gilbert damping with increasing thickness of the MgO capping layer comes from the interfacial effect, so we focus on the interface-enhancement part.

III. GILBERT DAMPING IN Ag/MgO-CAP/Fe MTJS

We consider an Ag/MgO(x nm)/Fe MTJ, as shown in Fig. 1, where the MgO-barrier thickness x ranges from 0 to 1.4 nm. In our calculation, we choose bcc Fe as one lead with the lattice constant $a_{\mathrm{Fe}} = 2.866$ Å, and the crystal MgO is reduced 4% and rotated 45 to match the bcc Fe. The lattice constant of fcc Ag is $a_{\mathrm{Ag}} = 4.053$ Å, and Ag is matched with MgO. The interlayer spacing between the Ag monolayer and the MgO surface layer is 2.52 Å for Ag above the O site [33], For the clean junction, we use a $400 \times 400k$-point mesh in the full two-dimensional Brillouin zone (BZ) to ensure numerical convergence. For the disordered interface case, we use a $40 \times 40k$-point mesh in the full two-dimensional BZ for a 4×4 lateral supercell, and 12 configurations are used to ensure configuration convergence. The scattering matrix is obtained using a first-principles wave-function method with tight-binding linearized muffin-tin orbitals [34].

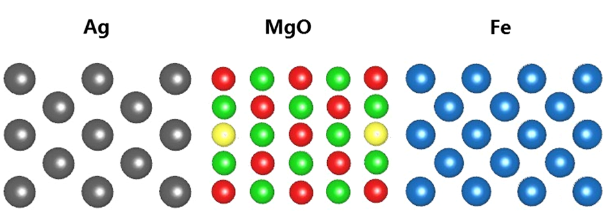

FIG. 1. Schematic Ag/MgO-cap(001)/Fe MTJs with five MgO monolayers. The red and green atoms in the scattering region (MgO) denote O and Mg, the gray atoms on the left leads denote Ag, and the blue atoms denote Fe. There are some oxygen vacancies (OVs, yellow) at the two interfaces.

First, we check how the MgO capping layer and MgO barrier affect $G^{\uparrow\downarrow}$. We study Ag/MgO-cap(n ML)/Fe(18 ML)/MgO-barrier(m ML)/Fe MTJs, where the MgO capping layer is n ML and the MgO barrier is m ML. Table I shows the dependences of $G^{\uparrow\downarrow}$ and TMR on the thickness of the MgO capping layer and MgO barrier. When considering the dependence of $G^{\uparrow\downarrow}$ and TMR on n (m), we fix m (n) equal to 3. The TMR is defined in terms of the conductance of the magnetization between the two Fe layers parallel (P) and antiparallel (AP): TMR $= [(G_P - G_{\mathrm{AP}})/G_{\mathrm{AP}}] \times 100\%$.

Table I shows that $G^{\uparrow\downarrow}$ decreases with increasing thickness of the MgO capping layer and does not change significantly with an increasing thickness of the MgO barrier. Gilbert damping is estimated from $G^{\uparrow\downarrow}$. As we show in Fig. 2, the experimental measurement of $G^{\uparrow\downarrow}$ is dominated by the MgO capping layer. Thus, we can choose the Ag/MgO-cap/Fe structure to study how the MgO capping layer affects the Gilbert damping of Ag/MgO-cap/Fe/MgO-barrier/Fe MTJs.

The MgO capping layer and MgO barrier have a different effect on the TMR. The TMR decreases with increasing thickness of the MgO capping layer and increases with an increasing thickness of the MgO barrier, which agrees with previous experiments [25].

Based on scattering theory, α is proportional to $G_r^{\uparrow\downarrow}$, which is related to the in-plane part of the spin current. We estimate α from Eq. (2). Figure 2 shows the α dependences of the MgO capping layer thickness of Ag/MgO(x nm)/Fe MTJs with 6.25% OVs at all Fe/MgO and Ag/MgO interfaces, with the thickness of the MgO capping layer ranging from 0 to 1.4 nm. α decays exponentially (inset of Fig. 2) with the thickness of the MgO capping layer.

TABLE I. Dependences of the spin-mixing conductance ($G^{\uparrow\downarrow}$) (in units of $10^{13}\ \Omega^{-1}\,\mathrm{m}^{-2}$) and the TMR on the thickness of the MgO capping layer with a 3-ML MgO barrier and on the thickness of the MgO barrier with a 3-ML MgO capping layer in Ag/MgO-cap(n ML)/Fe(18 ML)/MgO-barrier(m ML)/Fe MTJs with a clean interface and an interface with 6.25% OVs (in brackets). n is the number of MgO layers.

n ($m = 3$)	$G_r^{\uparrow\downarrow}$	$G_i^{\uparrow\downarrow}$	TMR (%)
2	1.991(4.252)	0.772(1.174)	1027.5(97.1)
3	0.119(0.315)	0.119(0.289)	449.5(29.1)
4	0.009(0.056)	0.016(0.051)	321.0(31.5)
5	0.002(0.011)	0.003(0.014)	209.1(2.88)
m ($n = 3$)			
2	0.158(0.380)	0.145(0.298)	245.2(1.10)
3	0.119(0.315)	0.119(0.289)	449.5(29.1)
4	0.099(0.314)	0.105(0.297)	918.9(91.2)
5	0.091(0.314)	0.101(0.233)	1288.3(97.4)

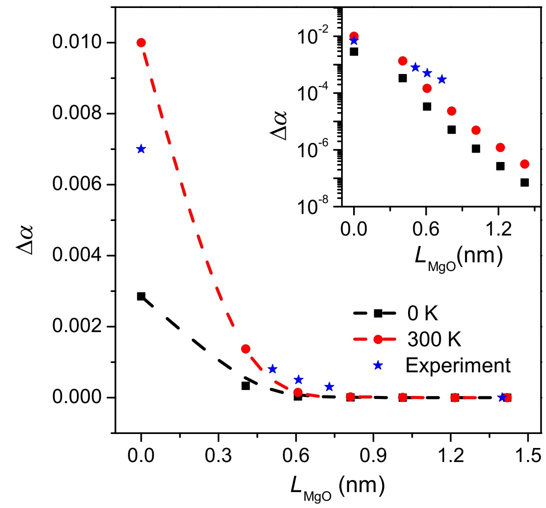

FIG. 2. Gilbert damping parameter in Ag/MgO(0–1.4 nm)/Fe MTJs as a function of MgO thickness in the presence of 6.25% OVs at the Fe/MgO and Ag/MgO interfaces at $T = 0$ and 300 K. $L_{\mathbf{MgO}} = 0$ nm is calculated from the Ag/Fe interface. For the case at 0 K, we assume 16-ML Fe (about 2 nm). $\Delta\alpha = \alpha(x)$-$\alpha(x = \infty)$. α is estimated from Eq. (2), and the temperature effect is considered including both the Fermi-Dirac distribution and the magnetic coherent volume effect. The blue stars are the experimental values [21] of the Ta/MgO(0–1.9 nm)/$Fe_{80}B_{20}$/MgO(1 nm)/Ta MTJs. The inset picture is the logarithmic coordinates for the y axis.

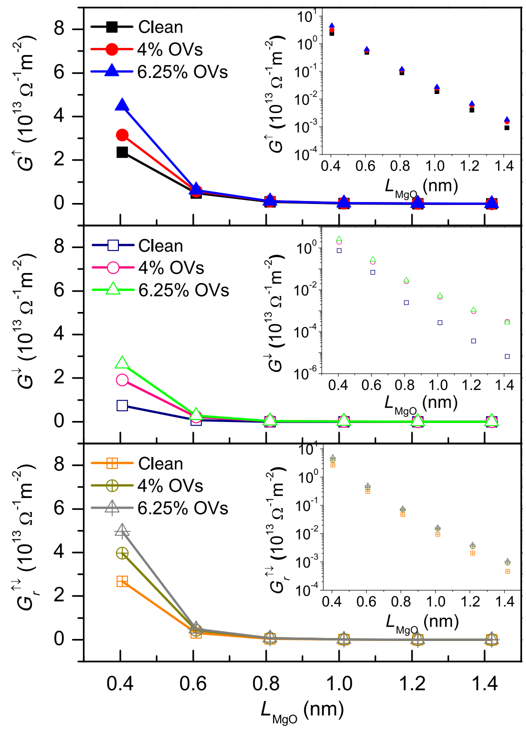

FIG. 3. Spin-dependent conductance $G^{\uparrow}$, $G^{\downarrow}$ (in units of $10^{13}\ \Omega^{-1}\,\mathrm{m}^{-2}$) and $G_r^{\uparrow\downarrow}$ (in units of $10^{13}\ \Omega^{-1}\,\mathrm{m}^{-2}$) in Ag/MgO(0–1.4 nm)/Fe MTJs as a function of MgO thickness in the presence of a clean interface, 4% OVs, and 6.25% OVs at the Fe/MgO and Ag/MgO interfaces. $G^{\uparrow}$, $G^{\downarrow}$, and $G_r^{\uparrow\downarrow}$ decrease with thickening of the MgO capping layer, and the results at the rough interface are larger than at the clean interface. α is estimated from $G_r^{\uparrow\downarrow}$.

$\Delta\alpha = 0.0029$ at $T = 0$ K and $\Delta\alpha = 0.01$ at $T = 300$ K, the second result of which is comparable to earlier experimental results [21] $\Delta\alpha = 0.007$ at room temperature in Ta/MgO(0–1.9 nm)/$Fe_{80}B_{20}$/MgO(1 nm)/Ta MTJs. As shown in Fig. 2, α decreases as the MgO capping layer thickens, which agrees well with the experiment. The good agreement between our calculations and experimental results indicates that the decreases in α are related to the suppression of the spin-pumping effects through the FM/NM interface, with inserting MgO layers.

To understand why α decreases as the MgO capping layer thickens, we compare the spin-dependent conductance $G^{\uparrow}$, $G^{\downarrow}$ $[G^{\uparrow(\downarrow)} = (e^2/h)\mathrm{Tr}(\mathbf{t}^{\dagger}_{\uparrow(\downarrow)}\mathbf{t}_{\uparrow(\downarrow)})]$ and $G_r^{\uparrow\downarrow}$ for various thicknesses of the MgO capping layer, as shown in Fig. 3. $G^{\uparrow}$, $G^{\downarrow}$, and $G_r^{\uparrow\downarrow}$ of the sample with the thinnest MgO layer are much larger than those of the thicker sample, showing an exponential decay as a function of MgO thickness (inset of Fig. 3). α is estimated from $G_r^{\uparrow\downarrow}$, and these results indicate that the decrease in α is related to the decrease in spin-dependent conductance.

We plot the $\mathbf{k}_{\parallel}$-resolved transmission and $G_r^{\uparrow\downarrow}$ at the Fermi energy for the epitaxial Ag/MgO(3 ML)/Fe MTJs with a clean interface, as shown in Figs. 4(a)–4(c). The logarithm function is applied to the transmission coefficient, and the red (blue) color represents a high- (low-) transmission probability. We find that the majority-spin channel mainly comes from $\mathbf{k}_{\parallel}$ points near the Γ point and that the minority-spin channel comes from bright $\mathbf{k}_{\parallel}$ points near the boundary of the BZ. The $G_r^{\uparrow\downarrow}$ channel contains features of both the majority and minority spins, indicating that $G_r^{\uparrow\downarrow}$ is related to spin-dependent conductance. The $G_r^{\uparrow\downarrow}$ channel in some k points is larger than 1, such as $G_r^{\uparrow\downarrow} = 1.99$ at $k_x a_0 = 0.7645$ and $k_y a_0 = 2.8926$, as shown with red circles in Fig. 4(c), where $a_0 = 0.286$ nm is the lattice constant of Fe. These large $G_r^{\uparrow\downarrow}$ channels are caused by the resonant states at those k points.

To understand how the interface roughness affects α, we study $G^{\uparrow}$, $G^{\downarrow}$, and $G_r^{\uparrow\downarrow}$ with clean 4% OVs and 6.25% OVs at the Fe/MgO and Ag/MgO interfaces, as shown in Fig. 3. $G^{\uparrow}$, $G^{\downarrow}$, and $G_r^{\uparrow\downarrow}$ are larger for the Fe/MgO and Ag/MgO interfaces with OVs than for the clean interfaces. The values increase at a higher concentration of OVs. This result agrees with previous studies of FeCo/MgO/FeCo MTJs [35].

As shown in Fig. 5, the origin of the increment of $G^{\uparrow}$ and $G^{\downarrow}$ for Fe/MgO and Ag/MgO interfaces with OVs that the transmission channels spread much wider into the BZ due to the diffusive scattering with interface roughness. Thus,

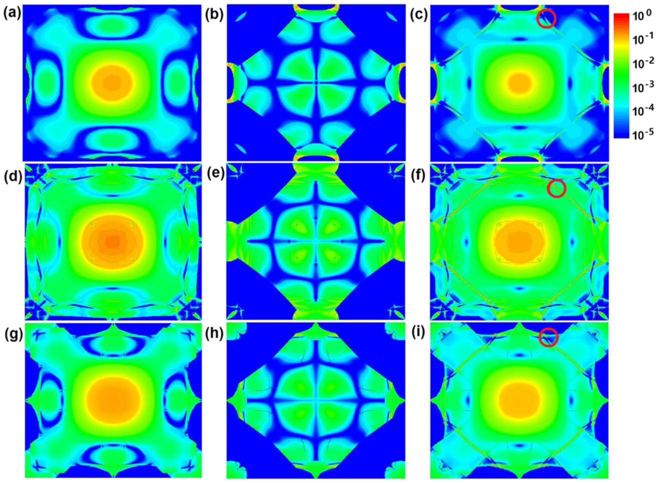

FIG. 4. $\mathbf{k}_{\parallel}$-resolved electron transmission probability for (a)–(c) Ag/MgO(3 ML)/Fe with a clean interface, (d)–(f) Ir/MgO(3 ML)/Fe with a clean interface, and (g)–(i) Pt/MgO(3 ML)/Fe with a clean interface at the Fermi energy: (a),(d),(g) for majority-spin ($G^{\uparrow}$) channels, (b),(e),(h) for minority-spin channels ($G^{\downarrow}$), and (c),(f),(i) for $G_r^{\uparrow\downarrow}$ channels. Resonant tunnel reflection features are shown with red circles.

the $G^{\uparrow}$ and $G^{\uparrow}$ after integrating over the entire BZ is larger for the rough interface than for the clean interface. $G_r^{\uparrow\downarrow}$ is determined by the coupling between the incoming states (arriving to interface) and magnetizations. The diffusion scattering enhances the conductance electrons, which also enhances the $G_r^{\uparrow\downarrow}$ and α for interfaces with OVs, so the clean interface is better for decreasing smaller α.

The ferromagnetic alloys FeCo and FeCoB are mostly used as spin sources in MgO-based multilayer structures because of their perpendicular magnetic anisotropy. Table II lists the parameters $G^{\uparrow}$, $G^{\downarrow}$, $G_r^{\uparrow\downarrow}$, and α for FeCo/MgO MTJs. We consider two kinds of structures: crystalline and alloy FeCo structures. The crystalline FeCo structure consists of alternating Fe and Co atomic layers along bcc (001), which can form a Fe- (Co-) terminated interface with MgO referred to as the "Fe (Co) term." For the alloy structure, Fe and Co in every layer (including the

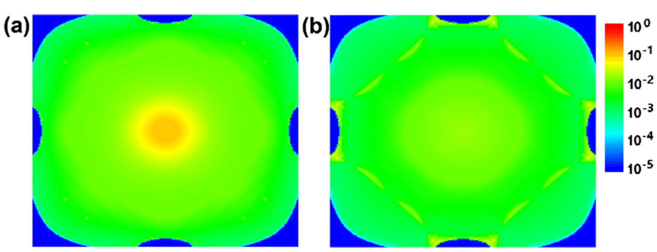

FIG. 5. $\mathbf{k}_{\parallel}$-resolved electron transmission probability for Ag/MgO(3 ML)/Fe with 6.25% OVs at both the Fe/MgO and Ag/MgO interfaces: (a) majority-spin ($G^{\uparrow}$) channels, (b) minority-spin ($G^{\downarrow}$) channels. This calculation for electron transmission probability is based on the Keldysh nonequilibrium Green's function [35,36].

TABLE II. Spin-dependent conductances $G^{\uparrow}$, $G^{\downarrow}$, $G_r^{\uparrow\downarrow}$ (in units of $10^{13}\ \Omega^{-1}\,\mathrm{m}^{-2}$) and α ($T = 300$ K) in Ag/MgO(n ML)/FM MTJs with clean interfaces. FM indicates Fe, crystalline, and alloy FeCo structures. Fe term (Co term) indicates that MgO is attached to both Fe (Co) layers of the crystalline FeCo. n is the number of MgO layers, and $n = 3$ is about 0.61 nm.

n	FM	$G^{\uparrow}$	$G^{\downarrow}$	$G_r^{\uparrow\downarrow}$	$\alpha(10^{-3})$
2	Fe	2.37	0.74	2.67	0.652
	$Fe_{0.25}Co_{0.75}$	2.32	0.50	1.61	0.455
	$Fe_{0.5}Co_{0.5}$	2.37	0.65	1.64	0.460
	$Fe_{0.75}Co_{0.25}$	2.40	0.96	1.89	0.527
	Fe term	2.63	0.31	1.80	0.532
	Co term	2.07	0.04	1.22	0.346
3	Fe	0.49	0.07	0.31	0.086
	$Fe_{0.25}Co_{0.75}$	0.47	0.05	0.27	0.077
	$Fe_{0.5}Co_{0.5}$	0.48	0.05	0.27	0.081
	$Fe_{0.75}Co_{0.25}$	0.51	0.06	0.29	0.083
	Fe term	0.52	0.03	0.29	0.085
	Co term	0.41	0.003	0.22	0.063

interface layer) are randomly distributed, and we consider three different compositions of Fe_xCo_{1-x}, where x is the concentration of Fe.

The magnetization of Co is smaller than that of Fe, so the total magnetization M_sV is different between Fe and FeCo. The total magnetizations are 2.36, 2.31, 2.18, 1.98, 2.27, and 2.22μ_B in Fe, $Fe_{0.75}Co_{0.25}$, $Fe_{0.5}Co_{0.5}$, $Fe_{0.25}Co_{0.75}$, Fe term, and Co term, respectively, for 1-ML ferromagnetic layers, where μ_B is the Bohr magneton.

Table II shows that the spin-dependent conductance and $G_r^{\uparrow\downarrow}$ are larger in junctions with Fe as the lead. Both crystalline and alloy FeCo decrease the value of α to lower than that with a Fe lead at $T = 300$ K. When Fe and Co atoms form an alloy, the interfacial resonant states are suppressed by the random distribution of atoms at the interface, reducing α. The value of α for Co term is smaller than for all the other structures. For example, for $2L$ MgO layers, $\alpha = 0.346$ in the Co-term crystalline FeCo structure, which is about 47% smaller than that for the Fe lead. These

TABLE III. $G_r^{\uparrow\downarrow}$, $G_i^{\uparrow\downarrow}$ (in units of $10^{13}\ \Omega^{-1}\,\mathrm{m}^{-2}$) dependence on MgO thickness in Fe/MgO/Ag MTJs with a clean interface and with 6.25% OVs at both the Fe/MgO and Ag/MgO interfaces (in brackets). n is the number of MgO layers and $L_{\mathbf{MgO}}$ is the corresponding distance in nanometers. The last row Fe/Ag is $n = 0$.

n	$L_{\mathbf{MgO}}$ (nm)	$G_r^{\uparrow\downarrow}$	$G_i^{\uparrow\downarrow}$
2	0.41	2.6731(4.9641)	0.6191(0.7751)
3	0.61	0.3144(0.4907)	0.1977(0.2373)
4	0.81	0.0474(0.0750)	0.0378(0.0553)
5	1.01	0.0096(0.0162)	0.0088(0.0142)
6	1.22	0.0021(0.0040)	0.0020(0.0040)
7	1.42	0.0005(0.0011)	0.0005(0.0011)
Fe/Ag	0	45.81	−0.11

TABLE IV. The calculated $G^{\uparrow}$, $G^{\downarrow}$, and $G_r^{\uparrow\downarrow}$ (in units of $10^{13}\ \Omega^{-1}\,\mathrm{m}^{-2}$) in NM/MgO($n$ ML)/Fe MTJs with a clean interface. NM is Ir, Pt, and Ag; n is the number of MgO layers.

n	NM	$G^{\uparrow}$	$G^{\downarrow}$	$G_r^{\uparrow\downarrow}$
2	Ir	5.01	2.55	9.33
	Pt	3.67	0.78	3.71
	Ag	2.37	0.74	2.67
3	Ir	1.24	0.09	0.88
	Pt	0.86	0.04	0.52
	Ag	0.49	0.07	0.31

results indicate that the FeCo lead is better for reducing α, especially for the Co-term crystalline FeCo structure.

From Eq. (1), $G_i^{\uparrow\downarrow}$ is related to the out-of-plane part of the spin current. The out-of-plane spin current can be ignored at the NM/FM interface because $G_i^{\uparrow\downarrow}$ is 2 orders of magnitude smaller than $G_r^{\uparrow\downarrow}$ (the value for the Fe/Ag interface in Table III). Our results indicate that the out-of-plane part of the spin current cannot be neglected compared with the in-plane part in the MgO-based MTJs, especially with a thick MgO capping layer (see Table III).

$G_i^{\uparrow\downarrow}$ modifies the gyromagnetic ratio and the frequency of ferromagnetic resonance [37]: $(1/\gamma_{\mathrm{eff}}) = (1/\gamma) \times \{1 - [(\hbar\gamma G_i^{\uparrow\downarrow})/(4\pi M_s V)]\}$, the frequency $\omega = \gamma H_{\mathrm{eff}}$, the change of the frequency is $\Delta\omega = [1/(1 - \hbar\gamma G_i^{\uparrow\downarrow}/4\pi M_s V) - 1]\omega$. In our calculations, $G_i^{\uparrow\downarrow} = 0.78 \times 10^{13}\ \Omega^{-1}\,\mathrm{m}^{-2}$ for 2-ML MgO with 6.25% OVs roughness at both interfaces, the frequency of the resonances in the MgO-based MTJ is about $\omega = 2$–14 GHz [38], which modifies the frequency by $\Delta\omega = 0.46$–3.22 MHz at room temperature and should be able to be observed experimentally.

To understand the effects of capping NMs, we study various NMs on the MgO/Fe interface. Table IV lists the calculated $G^{\uparrow}$, $G^{\downarrow}$, and $G_r^{\uparrow\downarrow}$ in NM/MgO(n ML)/Fe MTJs with a clean interface. We consider Ir, Pt, and Ag as NMs for 2- and 3-ML MgO layers. We choose fcc Pt (Ir) with the lattice constant $a_{\mathrm{Pt}} = 3.9242$ Å ($a_{\mathrm{Ir}} = 3.839$ Å). The in-plane lattice constant of the NM is matched with MgO, and the interlayer spacing between the NM monolayer and the MgO surface layer is 2.364 (2.305) Å for Pt (Ir) above the O site to ensure the space fulfilling.

We find that both spin-dependent conductance and $G_r^{\uparrow\downarrow}$ in Ir/MgO/Fe structures are higher than in Pt/MgO/Fe and Ag/MgO/Fe. To understand the difference, we plot the $\mathbf{k}_{\parallel}$-resolved transmission and $G_r^{\uparrow\downarrow}$ for Ir/MgO(3 ML)/Fe and Pt/MgO(3 ML)/Fe MTJs at the Fermi energy, as shown in Figs. 4(d)–4(i). $G_r^{\uparrow\downarrow}$ is dominated by the area near the Γ point of the 3-ML MgO barrier, and the transmission probability and area are larger in Ir than in Pt and Ag as a NM. The band structures along the fcc (001) of Ag, Ir, and Pt are analyzed in the following to further understand their difference, as shown in Fig. 6. The main contribution to the transmission channel is the Δ_1 state of MgO-based MTJs [3]. The kinetic energy in the Ir junction is larger than in Pt and Ag at the Fermi energy, so $G_r^{\uparrow\downarrow}$ is larger in Ir/MgO/Fe MTJs.

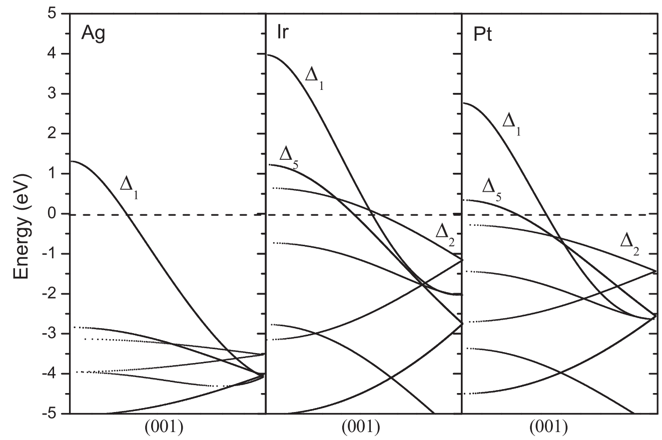

FIG. 6. Band structures of Ag, Ir, and Pt along (001), with the Fermi level fixed at 0 eV (indicated by the dotted line).

Table IV shows that $G_r^{\uparrow\downarrow}$ is larger than the spin-dependent conductance of Ir/MgO(2 ML)/Fe junctions. The relative spin-mixing conductance [39] $\eta = 2G_r^{\uparrow\downarrow}/(G^{\uparrow} + G^{\downarrow}) = 2.5$. The large η implies a large skewness of the angular-dependent STT of Fe/MgO/Ir structures, which makes this material promising for applications in high-frequency generators [40].

IV. SUMMARY

We estimate $G^{\uparrow\downarrow}$ in Ag/MgO(n ML)/Fe MTJs. At room temperature, our calculated α is consistent with the experimental results. The decrease in α is related to the suppression of spin-pumping effects in the Fe/Ag interface caused by inserted MgO layers. Our calculations show that both the interface roughness and site disorder in the ferromagnetic layer affect α, while a clean interface and alloy electrode are better for obtaining smaller α.$G_i^{\uparrow\downarrow}$ is nearly equal to $G_r^{\uparrow\downarrow}$ in the MgO-based MTJs, and the capping NM material affects α.

ACKNOWLEDGMENTS

We gratefully acknowledge financial support from the National Natural Science Foundation of China (Grants No. 61376105 and No. 21421003).

[1] S. S. Parkin, C. Kaiser, A. Panchula, P. M. Rice, B. Hughes, M. Samant, and S.-H. Yang, Giant tunnelling magnetoresistance at room temperature with MgO (100) tunnel barriers, Nat. Mater. 3, 862 (2004).

[2] S. Yuasa, T. Nagahama, A. Fukushima, Y. Suzuki, and K. Ando, Giant room-temperature magnetoresistance in single-crystal Fe/MgO/Fe magnetic tunnel junctions, Nat. Mater. **3**, 868 (2004).

[3] W. H. Butler, X.-G. Zhang, T. C. Schulthess, and J. M. MacLaren, Spin-dependent tunneling conductance of Fe|MgO|Fe sandwiches, Phys. Rev. B **63**, 054416 (2001).

[4] J. Mathon and A. Umerski, Theory of tunneling magnetoresistance of an epitaxial Fe/MgO/Fe(001) junction, Phys. Rev. B **63**, 220403 (2001).

[5] S. Ikeda, J. Hayakawa, Y. Ashizawa, Y. M. Lee, K. Miura, H. Hasegawa, M. Tsunoda, F. Matsukura, and H. Ohno, Tunnel magnetoresistance of 604% at 300 K by suppression of Ta diffusion in CoFeB/MgO/CoFeB pseudo-spin-valves annealed at high temperature, Appl. Phys. Lett. **93**, 082508 (2008).

[6] L. Jiang, H. Naganuma, M. Oogane, and Y. Ando, Large tunnel magnetoresistance of 1056% at room temperature in MgO based double barrier magnetic tunnel junction, Appl. Phys. Express **2**, 083002 (2009).

[7] S. Ikeda, K. Miura, H. Yamamoto, K. Mizunuma, H. Gan, M. Endo, S. Kanai, J. Hayakawa, F. Matsukura, and H. Ohno, A perpendicular-anisotropy CoFeB-MgO magnetic tunnel junction, Nat. Mater. **9**, 721 (2010).

[8] H. Sato, M. Yamanouchi, S. Ikeda, S. Fukami, F. Matsukura, and H. Ohno, Perpendicular-anisotropy CoFeB-MgO magnetic tunnel junctions with a MgO/CoFeB/Ta/CoFeB/MgO recording structure, Appl. Phys. Lett. **101**, 022414 (2012).

[9] C.-W. Cheng, W. Feng, G. Chern, C. M. Lee, and T. Wu, Effect of cap layer thickness on the perpendicular magnetic anisotropy in top MgO/CoFeB/Ta structures, J. Appl. Phys. **110**, 033916 (2011).

[10] D. D. Lam, F. Bonell, S. Miwa, Y. Shiota, K. Yakushiji, H. Kubota, T. Nozaki, A. Fukushima, S. Yuasa, and Y. Suzuki, Composition dependence of perpendicular magnetic anisotropy in Ta/$Co_xFe_{80-x}B_{20}$/MgO/Ta ($x = 0$, 10, 60) multilayers, J. Magn. **18**, 5 (2013).

[11] K. Yakushiji, A. Fukushima, H. Kubota, M. Konoto, and S. Yuasa, Ultralow-voltage spin-transfer switching in perpendicularly magnetized magnetic tunnel junctions with synthetic antiferromagnetic reference layer, Appl. Phys. Express **6**, 113006 (2013).

[12] A. Slavin and V. Tiberkevich, Nonlinear auto-oscillator theory of microwave generation by spin-polarized current, IEEE Trans. Magn. **45**, 1875 (2009).

[13] H. Kubota, K. Yakushiji, A. Fukushima, S. Tamaru, M. Konoto, T. Nozaki, S. Ishibashi, T. Saruya, S. Yuasa, Tomohiro Taniguchi, H. Arai, and H. Imamura, Spin-torque oscillator based on magnetic tunnel junction with a perpendicularly magnetized free layer and in-plane magnetized polarizer, Appl. Phys. Express **6**, 103003 (2013).

[14] S. Miwa, S. Ishibashi, H. Tomita, T. Nozaki, E. Tamura, K. Ando, N. Mizuochi, T. Saruya, H. Kubota, K. Yakushiji *et al.*, Highly sensitive nanoscale spin-torque diode, Nat. Mater. **13**, 50 (2014).

[15] J. C. Slonczewski, Current-driven excitation of magnetic multilayers, J. Magn. Magn. Mater. **159**, L1 (1996).

[16] X. Liu, W. Zhang, M. J. Carter, and G. Xiao, Ferromagnetic resonance and damping properties of CoFeB thin films as free layers in MgO-based magnetic tunnel junctions, J. Appl. Phys. **110**, 033910 (2011).

[17] S. Iihama, Q. Ma, T. Kubota, S. Mizukami, Y. Ando, and T. Miyazaki, Damping of magnetization precession in perpendicularly magnetized CoFeB alloy thin films, Appl. Phys. Express **5**, 083001 (2012).

[18] T. Devolder, P.-H. Ducrot, J.-P. Adam, I. Barisic, N. Vernier, J.-V. Kim, B. Ockert, and D. Ravelosona, Damping of $Co_xFe_{80-x}B_{20}$ ultrathin films with perpendicular magnetic anisotropy, Appl. Phys. Lett. **102**, 022407 (2013).

[19] L. Berger, Emission of spin waves by a magnetic multilayer traversed by a current, Phys. Rev. B **54**, 9353 (1996).

[20] S. Mangin, D. Ravelosona, J. A. Katine, M. J. Carey, B. D. Terris, and E. E. Fullerton, Current-induced magnetization reversal in nanopillars with perpendicular anisotropy, Nat. Mater. **5**, 210 (2006).

[21] M. Konoto, H. Imamura, T. Taniguchi, K. Yakushiji, H. Kubota, A. Fukushima, K. Ando, and S. Yuasa, Effect of MgO cap layer on Gilbert damping of FeB electrode layer in MgO-based magnetic tunnel junctions, Appl. Phys. Express **6**, 073002 (2013).

[22] S. Tsunegi, H. Kubota, S. Tamaru, K. Yakushiji, M. Konoto, A. Fukushima, T. Taniguchi, H. Arai, H. Imamura, and S. Yuasa, Damping parameter and interfacial perpendicular magnetic anisotropy of FeB nanopillar sandwiched between MgO barrier and cap layers in magnetic tunnel junctions, Appl. Phys. Express **7**, 033004 (2014).

[23] H. Kubota, S. Ishibashi, T. Saruya, T. Nozaki, A. Fukushima, K. Yakushiji, K. Ando, Y. Suzuki, and S. Yuasa, Enhancement of perpendicular magnetic anisotropy in FeB free layers using a thin MgO cap layer, J. Appl. Phys. **111**, 07C723 (2012).

[24] H. Yamamoto, J. Hayakawa, K. Miura, K. Ito, H. Matsuoka, S. Ikeda, and H. Ohno, Dependence of magnetic anisotropy in $Co_{20}Fe_{60}B_{20}$ free layers on capping layers in MgO-based magnetic tunnel junctions with in-plane easy axis, Appl. Phys. Express **5**, 053002 (2012).

[25] T. Takenaga, Y. Tsuzaki, C. Yoshida, Y. Yamazaki, A. Hatada, M. Nakabayashi, Y. Iba, A. Takahashi, H. Noshiro, K. Tsunoda, M. Aoki, T. Furukawa, H. Fukumoto, and T. Sugii, Magnetic tunnel junctions for magnetic field sensor by using CoFeB sensing layer capped with MgO film, J. Appl. Phys. **115**, 17E524 (2014).

[26] Y. Tserkovnyak, A. Brataas, and G. E. W. Bauer, Enhanced Gilbert Damping in Thin Ferromagnetic Films, Phys. Rev. Lett. **88**, 117601 (2002).

[27] Y. Tserkovnyak, A. Brataas, G. E. W. Bauer, and B. I. Halperin, Nonlocal magnetization dynamics in ferromagnetic heterostructures, Rev. Mod. Phys. **77**, 1375 (2005).

[28] T. Moriyama, R. Cao, X. Fan, G. Xuan, B. K. Nikolić, Y. Tserkovnyak, J. Kolodzey, and J. Q. Xiao, Tunnel Barrier Enhanced Voltage Signal Generated by Magnetization Precession of a Single Ferromagnetic Layer, Phys. Rev. Lett. **100**, 067602 (2008).

[29] A. Brataas, G. E. W. Bauer, and P. J. Kelly, Non-collinear magnetoelectronics, Phys. Rep. **427**, 157 (2006).

[30] A. Brataas, Y. Tserkovnyak, G. E. W. Bauer, and P. J. Kelly, Spin pumping and spin transfer, arXiv:1108.0385.

[31] J. Xiao, G. E. W. Bauer, K. C. Uchida, E. Saitoh, and S. Maekawa, Theory of magnon-driven spin Seebeck effect, Phys. Rev. B **81**, 214418 (2010).

[32] M. Weiler, M. Althammer, M. Schreier, J. Lotze, M. Pernpeintner, S. Meyer, H. Huebl, R. Gross, A. Kamra, J. Xiao, Y.-T. Chen, H. J. Jiao, G. E. W. Bauer, and S. T. B. Goennenwein, Experimental Test of the Spin Mixing Interface Conductivity Concept, Phys. Rev. Lett. **111**, 176601 (2013).

[33] O. Robach, G. Renaud, and A. Barbier, Structure and morphology of the Ag/MgO(001) interface during *in situ* growth at room temperature, Phys. Rev. B **60**, 5858 (1999).

[34] I. Turek, V. Drchal, J. Kudrnovský, M. Šob, and P. Weinberger, *Electronic Structure of Disordered Alloys, Surfaces and Interfaces* (Springer, New York, 1997).

[35] S.-Z. Wang, K. Xia, and G. E. W. Bauer, Thermoelectricity and disorder of FeCo/MgO/FeCo magnetic tunnel junctions, Phys. Rev. B **90**, 224406 (2014).

[36] Y. Ke, K. Xia, and H. Guo, Disorder Scattering in Magnetic Tunnel Junctions: Theory of Nonequilibrium Vertex Correction, Phys. Rev. Lett. **100**, 166805 (2008).

[37] M. Zwierzycki, Y. Tserkovnyak, P. J. Kelly, A. Brataas, and G. E. W. Bauer, First-principles study of magnetization relaxation enhancement and spin transfer in thin magnetic films, Phys. Rev. B **71**, 064420 (2005).

[38] J. C. Sankey, Y.-T. Cui, J. Z. Sun, J. C. Slonczewski, R. A. Buhrman, and D. C. Ralph, Measurement of the spin-transfer-torque vector in magnetic tunnel junctions, Nat. Phys. **4**, 67 (2008).

[39] A. Brataas, Y. V. Nazarov, and G. E. W. Bauer, Spin-transport in multi-terminal normal metal-ferromagnet systems with non-collinear magnetizations, Eur. Phys. J. B **22**, 99 (2001).

[40] J. C. Slonczewski, Currents and torques in metallic magnetic multilayers, J. Magn. Magn. Mater. **247**, 324 (2002).